Journal of Materials Research and Technology 35 (2025) 754–763

Contents lists available at ScienceDirect

Journal of Materials Research and Technology

journal homepage: www.elsevier.com/locate/jmrt

Strengthening nanostructured metals through dynamic recovery

Amanda P. Carvalho [a], Aoyan Liang [b], Megumi Kawasaki [c], Livia Cupertino-Malheiros [d], Paulo S. Branicio [b], Roberto B. Figueiredo [a,*]

[a] Department of Metallurgical and Materials Engineering, Universidade Federal de Minas Gerais, Belo Horizonte, MG, 31270-901, Brazil
[b] Mork Family Department of Chemical Engineering and Materials Science, University of Southern California, Los Angeles, CA, 90089, United States
[c] School of Mechanical, Industrial and Manufacturing Engineering, Oregon State University, Corvallis, OR, 97331, United States
[d] Department of Civil & Environmental Engineering, Imperial College London, London, SW7 2AZ, UK

ARTICLE INFO

Handling editor: SN Monteiro

Keywords:
Dynamic recovery
Deformation mechanism
Nanostructured metal
Molecular dynamics

ABSTRACT

Recovery plays distinct roles in nanostructured and coarse-grained metallic materials. While static and dynamic recovery usually soften work-hardened, coarse-grained materials, static recovery has been shown to strengthen nanostructured metals. This study extends this understanding by demonstrating that dynamic recovery can also strengthen nanostructured metals under deformation. Tensile, creep, and plane strain compression tests on nanostructured aluminum reveal a trend of increasing strain-hardening with decreasing strain rate and increasing temperature. Molecular dynamics simulations further indicate that sudden strain rate reductions lead to an initial drop in flow stress, followed by strain hardening. These findings suggest that dynamic recovery could serve as an effective strengthening mechanism for nanostructured metals, offering improvements in uniform elongation.

1. Introduction

There are many well-established strengthening mechanisms, including grain refinement, solid solution, second-phase particles, gradient structure, phase transformation, twinning, and strain hardening. Alloy compositions and thermo-mechanical processing routes have been developed to take full advantage of these mechanisms. While these mechanisms may enhance strength, only a few do so during deformation. This capability is crucial for maintaining stability during plastic deformation. Once the stress reaches a threshold and initiates plastic deformation, the volume undergoing deformation can maintain its strength, soften, or harden. If strength remains unchanged, deformation localization may develop, and this instability is exacerbated if the material softens. In the absence of strengthening during deformation, structural components can fail quickly due to deformation localization. For instance, uniform tensile deformation is only sustained if the material hardens during deformation, a process known as strain hardening.

Some mechanisms offer strengthening during plastic deformation. For example, deformation-induced twinning and phase transformation can strengthen the material and increase its ductility. However, these mechanisms are not easily accessible for most materials. Strain hardening through defect accumulation is a more common deformation-induced strengthening mechanism. It is readily available for most metallic materials and can significantly increase their strength. The underlying phenomenology has been extensively investigated [1]. Structural changes are well understood, and there are models that accurately predict material behavior. During plastic deformation, dislocations glide and may intersect other dislocations, creating immobile junctions and leaving dislocation debris within the grains. These defects act as barriers to other dislocations, increasing the stress required for further gliding. The greater the plastic deformation, the more barriers accumulate within the grains, forming dislocation substructures. Hardening would be continuous if not for the phenomenon of recovery. Dislocations can circumvent these barriers through cross-slip or climb processes, and the barriers can be removed by sufficient stress levels and/or thermal activation. This effect, known as recovery, can reduce the hardening rate and soften strain-hardened materials.

However, nanostructured materials behave differently. The grain size is too small to allow the buildup of a dislocation substructure. Dislocations are emitted from a grain boundary and glide unimpeded across the grain interior before being absorbed in the opposite boundary. Consequently, dislocation interaction during gliding is prevented, and these materials do not harden due to the accumulation of dislocation

* Corresponding author.
E-mail address: figueiredo@demet.ufmg.br (R.B. Figueiredo).

https://doi.org/10.1016/j.jmrt.2025.01.053
Received 11 November 2024; Received in revised form 24 December 2024; Accepted 7 January 2025
Available online 8 January 2025

barriers. The significant strength achieved by grain refinement hardening is thus coupled with the low ability of these materials to stretch in tension, known as the strength-ductility paradox [2,3]. It is important to note that nanostructured materials can display a different relationship between dislocation density and strength [4]. Static recovery through low-temperature annealing, which softens coarse-grained materials, can strengthen nanostructured counterparts. Many studies have shown this effect, although the explanations may vary. For instance, annealing hardening in nanostructured materials has been attributed to a reduction of internal stresses [5,6], changes in grain boundary structure [7–9], and/or a decrease in the density of crystal structure defects [8,10,11]. This effect has been reviewed in the literature [9,12]. The reduction of crystalline defects during unloaded annealing is considered static recovery. Recovery may also take place during deformation and in this case the stress and strain may contribute to the process in addition to the thermal contribution. The latter is considered dynamic recovery.

Given that static recovery can enhance the strength of a nanostructured material, we posit that dynamic recovery can strengthen it during deformation and assist with its stabilization. To prove this hypothesis, a nanostructured commercial purity aluminum (over 99% purity) processed by high-pressure torsion was subjected to various mechanical testing conditions to promote dynamic recovery.

2. Experimental procedure

Commercial purity (CP) aluminum (>99.0% purity) was used in this work. Discs of 8 mm diameter and 0.8 mm thickness were cut from rolled sheets and processed by quasi-constrained high-pressure torsion (HPT) at room temperature (~296 K) for 5 turns. The nominal pressure of HPT was 6 GPa, and the lower anvil rotated at 1 rpm. Some samples were annealed at 423 K for 15 min in order to evaluate any change in grain structure upon heating to this temperature. The microstructures of the as-processed and annealed samples were assessed by transmission electron microscopy (TEM) JEOL JEM-2100F. Samples for TEM observation were prepared in a double-jet electropolishing machine with an electrolyte of 25% vol. HNO_3 and 75% vol. methanol. The grain size was determined by the average of 150 individual grain sizes using dark-field and bright-field images.

The indentation creep test was used to estimate the strain rate sensitivity. The tests were conducted using an ultra-microhardness equipment model Shimadzu DUH-211S equipped with a Berkovich indenter. The loading rate was 70.1 mN/s, the maximum load was 300 mN, and the holding time was 600 s. The load, time, and depth were converted into effective stress and strain rates [13,14].

Tensile tests were carried out using miniature samples with 1.6 mm gauge length and 0.8 × 0.7 mm^2 cross-section. The samples were extracted from the HPT processed discs using spark erosion, and care was taken to avoid the area near the disc center. The tests were carried out using a constant rate of cross-head displacement and nominal initial strain rates in the range 10^{-5}–10^{-2} s^{-1}. Tests were carried out at room temperature and at 373 K. An additional test was carried out at 423 K with a strain rate of 10^{-4} s^{-1}. The strain rate was varied in an additional test to evaluate the transient stress vs. strain curve. Tensile creep tests were also performed using samples similar to the ones for tensile tests. A constant load was applied using a lever system, and a high-precision double LVDT (Linear Variable Differential Transformer) tracked the sample elongation. Creep tests were carried out considering different loads and at different temperatures. The elongation and time were converted to strain and strain-rate data considering homogeneous deformation of the sample. Plane Strain Compression (PSC) tests were used to estimate the stress vs. strain relationship at larger strain intervals. A special device for testing small HPT samples was used [15]. Tests were carried out considering constant and variable strain rates.

X-ray Diffraction (XRD) patterns were collected for the HPT processed material and for a sample subjected to straining at 10^{-6} s^{-1} using plane strain compression. The XRD machine used was a PANalytical C'Pert Pro diffractometer with a CuK_α radiation and a graphite monochromatic crystal with a wavelength of 1.5406 Å. MAUD software was used to estimate the crystallite size and microstrain through Rietveld refinement of the XRD pattern.

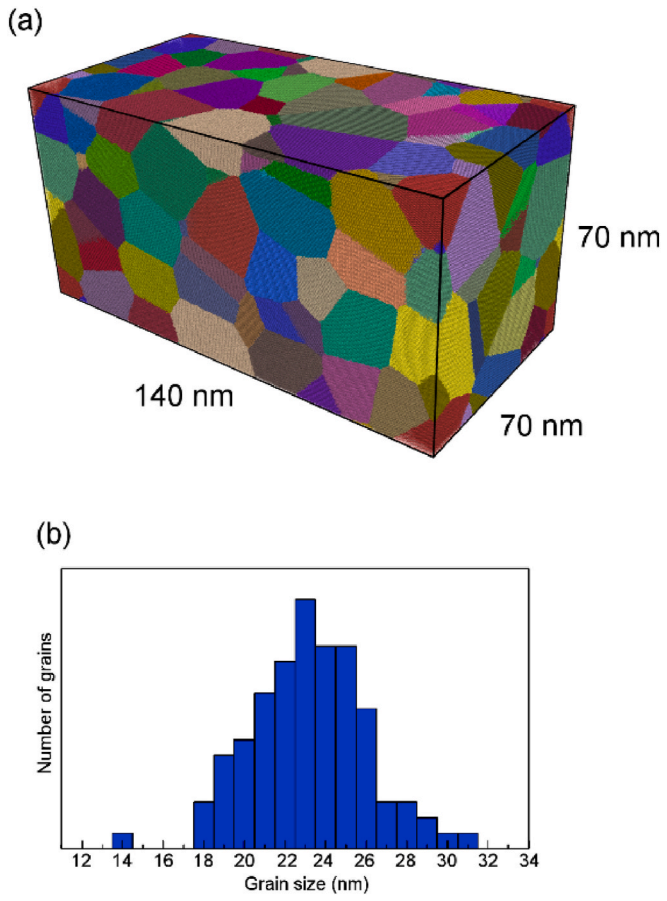

Fig. 1. Initial structure for molecular dynamics simulation of nanostructured aluminum. (a) Atomic model used in the molecular dynamics simulations, showing a 140 x 70 × 70 nm^3 box with 100 grains with random orientation. (b) Grain size distribution within the model, with most grains ranging from 18 to 31 nm and an average grain size of ~23 nm.

Molecular dynamics simulations were carried out using LAMMPS [16] package, considering EAM (Embedded Atom Model) potential for aluminum [17]. The initial structure was built using Atomsk software [18] and Voronoi tessellation method. An initial box with 140 × 70 × 70 nm^3 was built with 100 grains with random orientation and periodic boundary conditions. The number of atoms in the system was ~41,000,000. The grain sizes were mostly in the 18–31 nm range, and the average grain diameter was ~23 nm. The initial system is shown in Fig. 1a and the grain size distribution is shown in Fig. 1b. Overlapping atoms at grain boundaries were deleted. The system was equilibrated at 300 K and 0 GPa for 100 ps using Langevin thermostat and the isoenthalpic–isobaric (NPH) ensemble. After equilibration, the system was subjected to compression deformation along the longest axis of the box at a strain rate of 10^8 s^{-1} for up to 25% strain. Additional simulations were carried out starting from a deformation of 7.5% but considering abrupt changes in strain rate to 10^9 s^{-1} and 10^7 s^{-1}. These different strain rates were imposed during 5% straining, and then the strain rate was brought back to 10^8 s^{-1} and deformation proceeded for additional 10%. The structure was observed and analyzed using OVITO software [19].

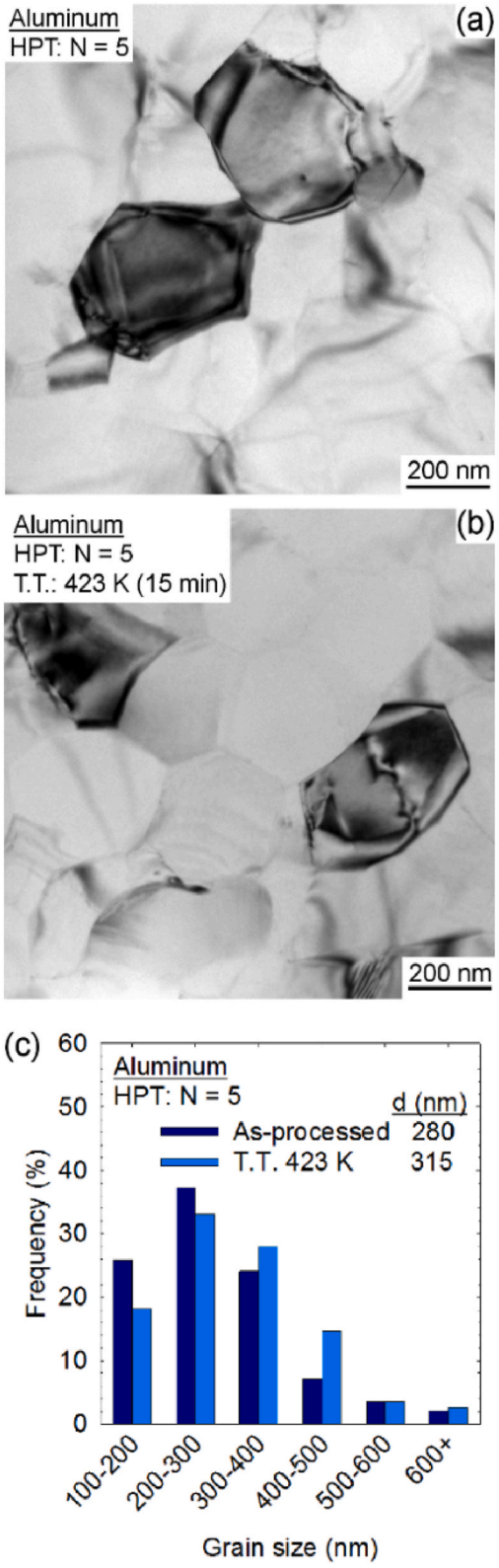

Fig. 2. Grain structure of nanostructured aluminum processed by high-pressure torsion (HPT). (a) Grain structure in the as-processed condition. (b) Grain structure after thermal treatment at 423 K for 15 min. (c) Grain size distribution for both conditions, showing average grain sizes of 280 nm (as-processed) and 315 nm (thermally treated).

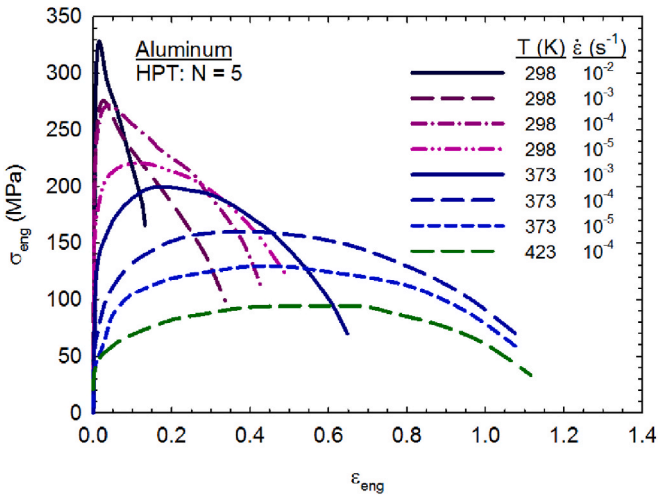

Fig. 3. Engineering stress vs. engineering strain curves for tensile tests conducted at various strain rates (10^{-2} to 10^{-5} s^{-1}) and temperatures (298 K, 373 K, and 423 K).

3. Results

3.1. Experiments

The grain structure of the processed material is shown in Fig. 2a, and that of the material heated to 423 K for 15 min is shown in Fig. 2b, revealing only minor changes. Grain measurements from multiple images are presented in Fig. 2c, indicating an average size of 280 nm in the as-processed material and 315 nm for the thermally treated counterpart, demonstrating that the structure remains stable up to 423 K.

Tensile tests were carried out at different strain rates and temperatures, with the engineering stress, σ_{eng}, vs. engineering strain, ε_{eng}, curves depicted in Fig. 3. The yield stress decreases with lower strain rates and higher temperatures, indicating significant thermal activation of plastic deformation. Notably, the shape of the curves changes, and elongation to failure improves substantially at low strain rates and higher temperatures. At high strain rates at room temperature, a peak stress is observed immediately upon yielding, followed by a continuous decrease in stress. Conversely, at the lowest strain rate at room temperature and at higher temperatures, yield is followed by a range of deformation under increasing stress until reaching the peak. This range of deformation under increasing stress is termed uniform elongation. The curves demonstrate that uniform elongation increases at low strain rates and higher temperatures, conditions that enhance dynamic recovery. After the peak stress, the slope of the softening portion of the curves also decreases. Thus, both the uniform and the post-uniform elongation increase with decreasing strain rate and increasing temperature.

Tensile creep tests were also used to evaluate the deformation behavior of the nanostructured aluminum. The evolution of the strain rate ($\dot{\varepsilon}$) as a function of the strain for three applied stresses is depicted in Fig. 4a. The curve obtained at the highest stress (250 MPa) displays a few percent plastic deformation until the minimum strain rate, followed by failure with less than 10% strain. In contrast, the curves for tests at lower stresses show decreasing strain rates with increasing deformation, suggesting material strengthening. Slower strain rates at lower stresses favor dynamic recovery, indicating that dynamic recovery strengthens the nanostructured aluminum. This effect stabilizes tensile deformation, preventing necking and allowing the samples to stretch before rupture. A creep test under 150 MPa stress was interrupted after 25% strain, and the stretched sample is shown in Fig. 4b. The gauge length does not exhibit any sign of necking, confirming that the elongation was uniform. This is a remarkable uniform elongation for nanostructured aluminum

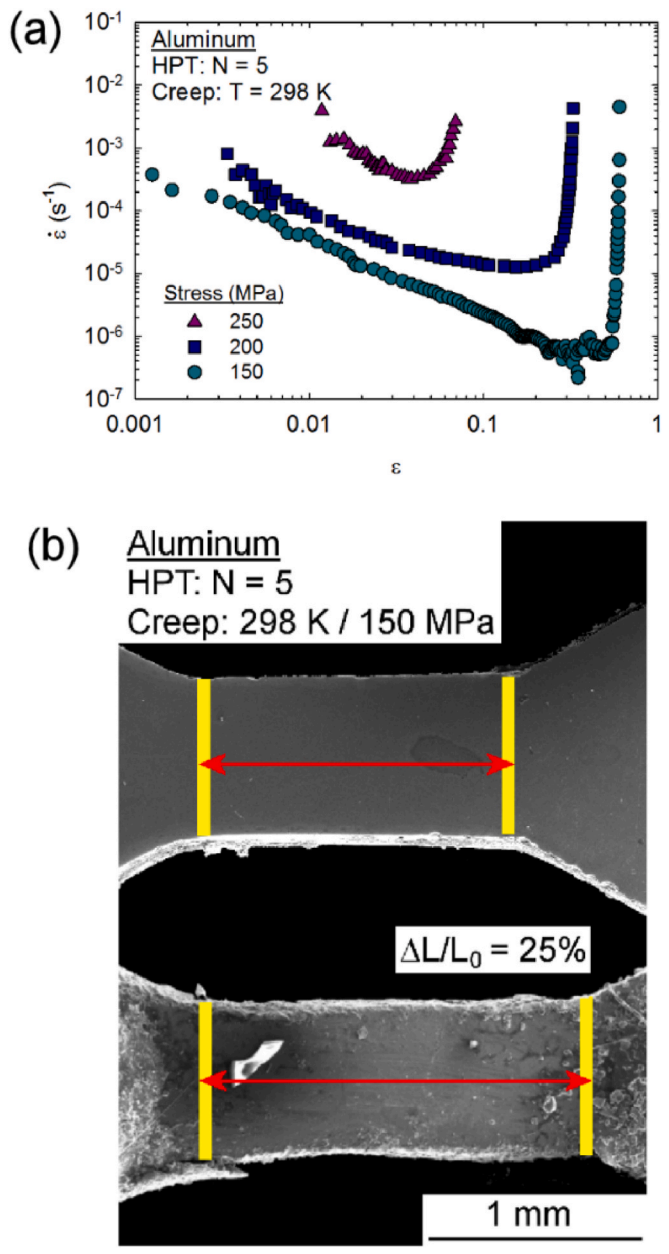

Fig. 4. Tensile creep behavior of nanostructured aluminum. (a) Strain rate vs. strain curves obtained in tensile creep tests at room temperature under different stresses. (b) Appearance of a creep sample before and after creep deformation to 25% elongation under 150 MPa.

deformed at room temperature.

The plane strain compression test was used to evaluate the relationship between effective stress, σ, and effective strain, ε, over a broader range of deformation. This test is appropriate for thin samples, such as those in the present study, and allows for stable plastic deformation of materials with low hardening. Stress vs. strain curves for the nanostructured aluminum tested at 10^{-3} s^{-1} and 10^{-6} s^{-1} are shown in Fig. 5a, along with the corresponding strain hardening parameter ($\Theta = \partial\sigma/\partial\epsilon$). The material tested at the higher strain rate displays a rapid elastic to plastic transition, with plastic deformation occurring under almost constant stress and negligible strain hardening ($\Theta \approx 0$ MPa). The sample tested at 10^{-6} s^{-1} exhibits much lower yield strength, and the plastic deformation occurs under increasing flow stress. The strain hardening parameter decreases during deformation but remains higher than observed at the faster strain rate.

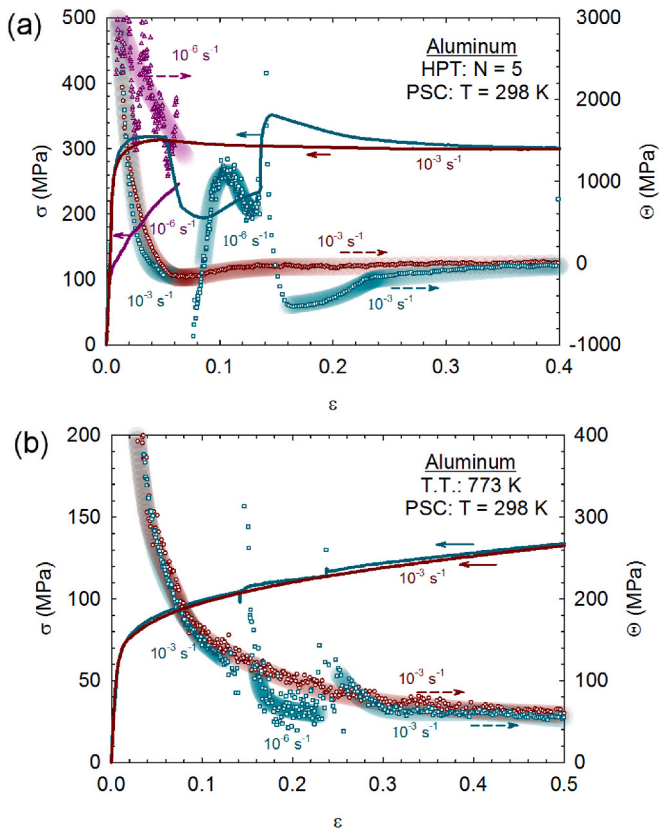

Fig. 5. Effective stress vs. effective strain and hardening vs. effective strain curves obtained in plane strain compression (PSC) tests of (a) the material processed by HPT and (b) the material annealed at 773 K for grain growth to ~10 μm.

To confirm the tendency of increasing strain hardening with decreasing strain rate, a test was conducted in which the strain rate was varied from 10^{-3} s^{-1} to 10^{-6} s^{-1} and back to 10^{-3} s^{-1}. As expected, plastic deformation occurs with negligible hardening at 10^{-3} s^{-1}. Decreasing the strain rate produces a sharp drop in flow stress, indicating significant strain rate sensitivity. However, the flow stress increases at 10^{-6} s^{-1} as deformation continues. The hardening at 10^{-6} s^{-1} becomes significantly higher than at 10^{-3} s^{-1}, which is contrary to expectations for coarse-grained materials. To clarify this difference, tests were conducted on a sample annealed at 773 K to coarsen the grain size to ~10 μm. The stress and hardening vs. strain curves of this sample are shown in Fig. 5b. The coarse-grained sample displays strain hardening behavior with a continuous decrease in the hardening parameter during deformation at 10^{-3} s^{-1}. A similar strain rate variation test was conducted on this sample. Reducing the strain rate from 10^{-3} s^{-1} to 10^{-6} s^{-1} produces a negligible change in the flow stress, indicating a lack of strain rate sensitivity. However, there is a noticeable decrease in the hardening coefficient at the lowest strain rate. This confirms that deformation at low strain rates, which favors dynamic recovery, decreases the hardening rate of coarse-grained aluminum, which is the opposite of what is observed in the nanostructured counterpart.

Another noteworthy observation during the plane strain compression test of the nanostructured aluminum (Fig. 5a) is that the hardening achieved at the lowest strain rate affects the flow stress of the material after the strain rate is increased. An increase in flow stress of over 10% is observed at 10^{-3} s^{-1} in the material previously strained at 10^{-6} s^{-1}. This suggests that the nanostructured material retains the hardening induced by dynamic recovery. However, a significant drop in flow stress occurs immediately after reaching the peak, and the flow stress gradually approaches the level observed during continuous testing at 10^{-3} s^{-1}.

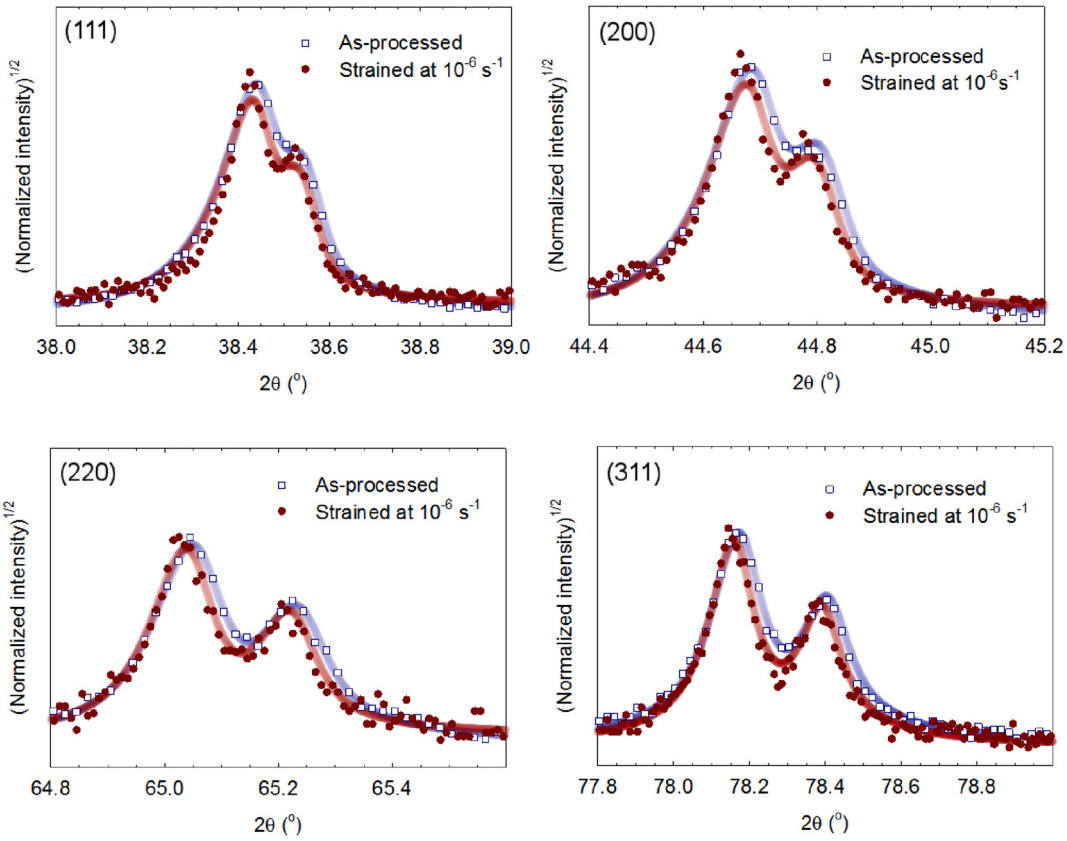

Fig. 6. Square root of the normalized intensity obtained by X-ray diffraction and Rietveld refinement of the as-processed material and the material strained at a low strain rate.

Table 1
Summary of crystalline size, D, microstrain, μ, and dislocation density, ρ, obtained from XRD analysis using Rietveld refinement for the material processed by HPT and the material strained at low strain rate.

	D (nm)	μ	ρ (m^{-2})
HPT processed	450	3.8×10^{-4}	1.0×10^{13}
HPT processed + 6% strain at 10^{-6} s^{-1}	670	1.0×10^{-4}	1.9×10^{12}

X-ray diffraction pattern analysis was used to support the assumption that dynamic recovery occurs in nanostructured material deformed at very low strain rates. The diffraction patterns of the as-processed material and the material deformed by plane strain compression at 10^{-6} s^{-1} are shown in Fig. 6. There is a clear reduction of the full-width half-maxima (FWHM) for all peaks in the latter. The crystallite size (D) and microstrain (μ) values obtained from the Rietveld refinement method are shown in Table 1, and it is observed that low strain rate deformation increases D and decreases μ. This suggests that the sample deformed at low strain rate experienced some grain growth. The dislocation density, ρ, was estimated using the relationship [20] below and the values are reported in Table 1.

$$\rho = \frac{2\sqrt{3}\sqrt{\mu^2}}{Db} \quad (1)$$

Where b is the Burgers vector. It is observed that the dislocation density is one order of magnitude smaller in the material deformed at low strain rate compared to the as-processed material.

It is now established that the strength of nanostructured materials can be enhanced by static recovery through annealing. Various groups have reported this phenomenon, with different explanations suggested [9]. These include a reduction of internal stresses [5,6], changes in grain boundary structure [7–9], grain boundary relaxation [21], and a decrease in the density of crystal structure defects [8,10,11,21]. A recent deformation mechanism for nanostructured materials, based on grain boundary sliding through dislocation glide, has been proposed [22]. It predicts that both a reduction in mobile dislocations and an increase in stress for dislocation emission from grain boundaries can increase flow stress. The former could reduce the dislocation pile-up length, and the latter directly affects the stress required for deformation.

The indentation creep test was used to estimate the strain rate sensitivity of the nanostructured aluminum. The effective stress is plotted as a function of the effective strain rate in Fig. 7a, and the data reveal a strain rate sensitivity of ~0.1. A creep test in which the temperature varied during deformation was also carried out on the nanostructured material. The data is shown in Fig. 7b, and the difference in strain rate at the different temperatures reveals an apparent activation energy of ~68 kJ/mol. Both the strain rate sensitivity and the activation energy agree with the predictions from the model of grain boundary sliding [22].

3.2. Molecular dynamics simulation

Molecular dynamics (MD) simulations were conducted to investigate the deformation behavior of nanocrystalline aluminum during changes in strain rate. The simulations used a model with an average grain size of approximately 23 nm, subjected to uniaxial compression at an initial strain rate of 10^8 s^{-1}. Additional simulations were performed with ten-fold variations in strain rates, both faster and slower, which were then returned to 10^8 s^{-1} after 0.05 strain. While MD simulations have limitations in sample size and strain rate compared to experimental conditions, they enable tracking of structural changes during plastic deformation. Specifically. MD simulations are typically limited to sample size on the order of tens to hundreds of nanometers and strain rates

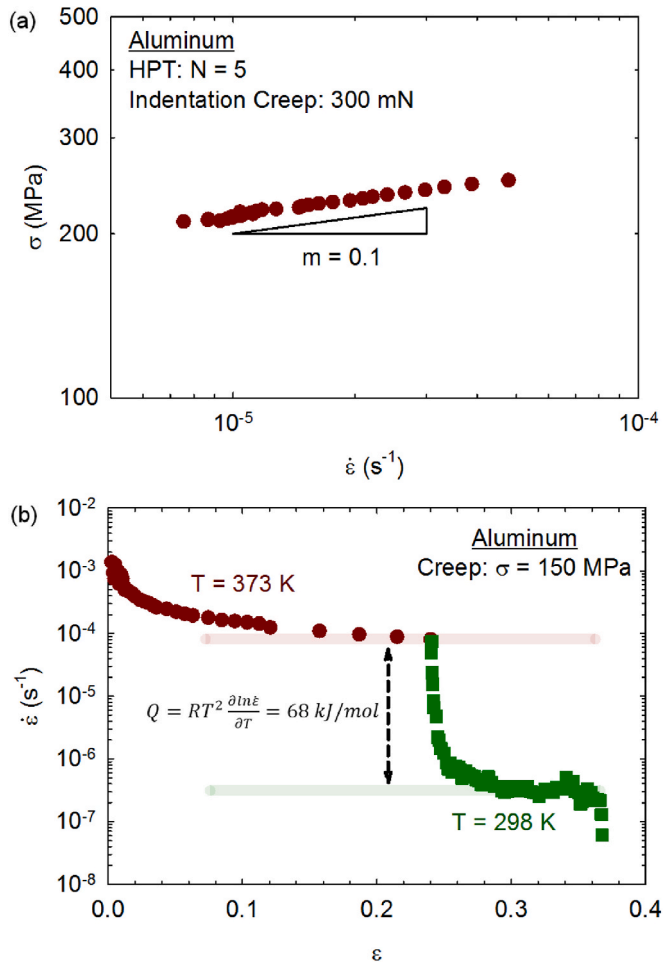

Fig. 7. (a) Effective stress estimated by indentation creep test plotted as a function of the strain rate and the estimated strain rate sensitivity. (b) The strain rate observed in the tensile creep test was plotted as a function of the strain. The temperature was changed in the test to estimate the apparent activation energy.

ranging from 10^6 to 10^{10} s^{-1}, which are usually several orders of magnitude higher than those in experimental conditions. These simulations were specifically designed to capture the effects of strain rate changes in nanocrystalline aluminum, using a grain size large enough to avoid the inverse Hall-Petch regime but small enough to prevent the buildup of dislocation substructures. It is important to note that the MD simulations do not reproduce the present experimental conditions. The MD simulations were carefully designed to balance computational feasibility with the need to capture key physical mechanisms under extreme conditions. Despite these differences, our simulations successfully reproduce trends consistent with experimental observations, demonstrating the robustness of the conclusions. Their aim is to show that dynamic recovery can indeed produce strengthening in nanocrystalline aluminum for a wide range of grain size and strain rate, and to provide insights regarding the structural changes taking place during transients in strain rates.

Fig. 8a shows the stress-strain curves for the simulations. A decrease in strain rate to 10^7 s^{-1} caused an immediate drop in flow stress due to a significant strain rate sensitivity, followed by a strain-hardening stage at the lowest strain rate. When the strain rate was returned to 10^8 s^{-1}, the flow stress increased to a level higher than that observed in the monotonic test, followed by gradual softening. The opposite effect occurred when the strain rate was increased. An increase in strain rate caused a pronounced rise in flow stress due to strain rate sensitivity, followed by a short-term softening at 10^9 s^{-1}. Returning the strain rate to 10^8 s^{-1} resulted in a sharp decrease in flow stress to a level lower than that in the monotonic test, followed by a hardening stage. These behaviors show some similarity to the experimental results on nanostructured aluminum discussed in the previous section, despite the smaller grain size and much higher strain rates in the simulations.

Representative images of the structure at a strain level of 0.125 for deformation at the fastest strain rate (10^9 s^{-1}) and at the lowest (10^7 s^{-1}) are shown in Fig. 8b. A notable observation from these images is the difference in grain boundary thickness. Atoms at grain boundaries, near dislocation cores and defects are not considered as atoms in perfect crystalline structure and are grouped as non-crystalline atoms. It is observed that the volume of atoms with non-crystalline structure increases with increasing strain rate.

Dislocations are identified using dislocation analysis (DXA) algorithm [23,24] and they are separated into different dislocation types including perfect dislocations, Shockley partials, stair-rod, Hirth and Frank. The densities of Shockley partials 1/6<112> were quantified at different deformation stages since this type of dislocation contributes the most to plastic deformation in FCC metals. The evolution of the non-crystalline volume (NCV) and the mobile Shockley partial 1/6<112> dislocation density is shown in Fig. 8c and d, respectively. The starting material exhibits a relatively low defect density, and these parameters increase during deformation. There is a significant increase in the non-crystalline fraction and dislocation density during deformation at the fastest strain rate of 10^9 s^{-1}. Conversely, there is a decrease during deformation at 10^7 s^{-1}, although the difference in mobile dislocation density between the material strained at 10^8 s^{-1} and at 10^7 s^{-1} is minimal. When the strain rate is returned to 10^8 s^{-1}, the defect density gradually approaches the level observed in the monotonic test. These observations confirm that some defects generated at faster strain rates are recovered during deformation at lower strain rates in nanocrystalline materials. It is important to note that the periods with a decrease in defect density (NCV and mobile dislocations) correspond to the periods with an increase in flow stress, confirming that dynamic recovery strengthens the nanocrystalline material. The grain boundary thickness appears to play a more important role than mobile dislocation density. A previous study [25] on nanocrystalline Ni using molecular dynamics showed that annealing brings the grain boundaries and triple junctions to a more equilibrium state, increasing the strength of the material, which aligns with the present analysis.

4. Discussion

The experimental results show distinct transients in stress-strain behavior. It is worth noting that the mechanical tests (tensile, creep and plane strain compression) in the present investigation were carried out in aluminum that had been pre-processed by severe plastic deformation. The high strain applied during high-pressure torsion likely exceeded the threshold needed for structural saturation in aluminum, suggesting that defect generation from straining was balanced by defect restoration [26]. Therefore, strain hardening from defect accumulation was largely exhausted. In fact, negligible strain-hardening was observed during tensile, creep or plane strain compression tests at strain rates of approximately 10^{-3} s^{-1} and faster at room temperature. Such strain rate is comparable to the strain rate during previous HPT processing ($\sim 10^{-1}$ s^{-1} at mid-radius in the present experiments). However, strain-hardening was observed in conditions favoring dynamic recovery, specifically at much lower strain rates and higher temperatures. These observations support the hypothesis that dynamic recovery could strengthen nanostructured materials.

The mechanism of dynamic recovery is not fully understood. The XRD analysis show an increase in crystallite size and a decrease in microstrain during low strain rate deformation of the nanostructured material. Thus, both effects suggest a decrease in the amount of crystalline defects and the assumption that dynamic recovery takes place during low strain rate deformation. MD simulations show that the

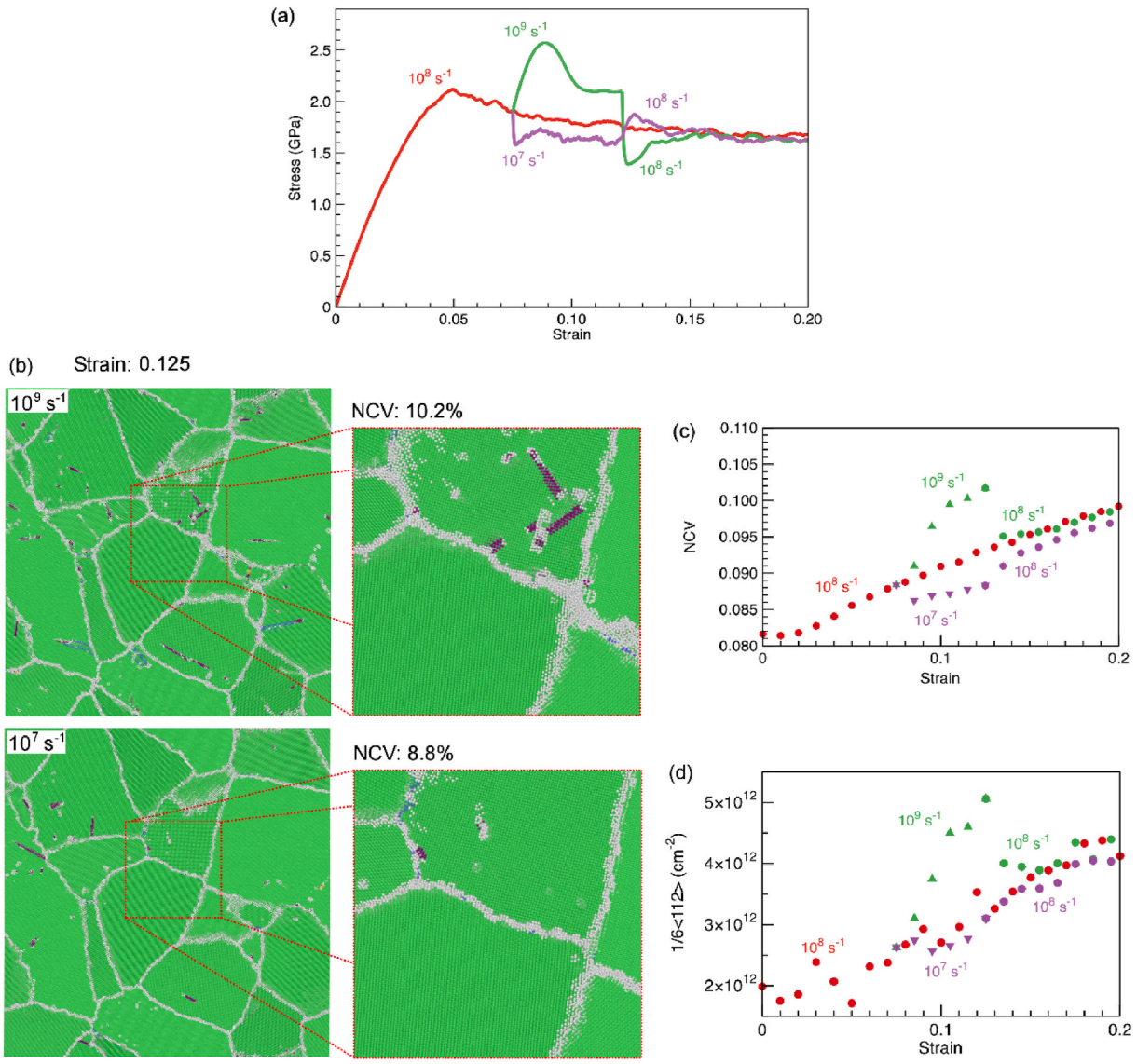

Fig. 8. Simulation of the deformation behavior of nanocrystalline aluminum under varying strain rates. (a) Stress vs. strain curves obtained during uniaxial compression tests. (b) Representative images of the structure at a strain of 12.5% during deformation at 10^9 s^{-1} and 10^7 s^{-1}. (c) Evolution of non-crystalline volume (NCV). (d) Evolution of mobile Shockley partial 1/6<112> dislocation density. Atoms in (b) are colored according to their crystalline structure: FCC (green), stacking faults (purple), coherent twins (blue), and non-crystalline (white).

amount of non-crystalline volume in nanocrystalline material depends on the strain rate. Thus, the lower the strain rate the lower the amount of non-crystalline volume. This is in line with the experimental observations despite the significant differences in grain size and strain rate between the experiments and the MD simulation. It also shows that changes in strain rate during deformation produces transients in flow stress response. In practice, if the nanocrystalline material has been previously deformed at a faster strain rate, the amount of non-crystalline volume is larger and the flow stress decreases. As the amount of non-crystalline volume reduces, the flow stress increases producing "strain-hardening". This suggests that the thickness of the grain boundary affects the stress required for grain boundary sliding, which plays a major role during plastic deformation of nanostructured materials. It is worth noting that MD simulation revealed that a significant portion of deformation is concentrated along grain boundaries.

Dynamic recovery hardening can be used to produce stronger materials, as confirmed in Fig. 9a, which shows experimental tensile stress vs. strain curves for tests at 10^{-3} s^{-1} and 10^{-2} s^{-1} in nanostructured aluminum in the as-processed condition and after being subjected to ~8% strain at a low strain rate of 10^{-5} s^{-1}. The low strain rate deformation favors dynamic recovery, and the nanostructured material becomes stronger upon reloading at a faster strain rate. However, softening occurs in the recovered material once the density of defects rises again during deformation at a faster rate, potentially compromising elongation.

The ultimate tensile strength and overall elongations observed in tensile tests at various strain rates and temperatures are plotted in Fig. 9b. The data for tests carried out at room temperature are depicted using dark red circles while the data for tests at 373 K are depicted using bright red circles. The results are compared to data from the literature [10,27–44] for tests at room temperature, showing that the nanostructured material displays increased strength when tested at room temperature and increased elongation when tested at 373 K. The high strength is attributed to grain refinement, with further strengthening achieved through dynamic recovery via pre-straining. The large elongations are attributed to high strain rate sensitivity values and strain hardening by dynamic recovery.

It is now well established that nanostructured materials display

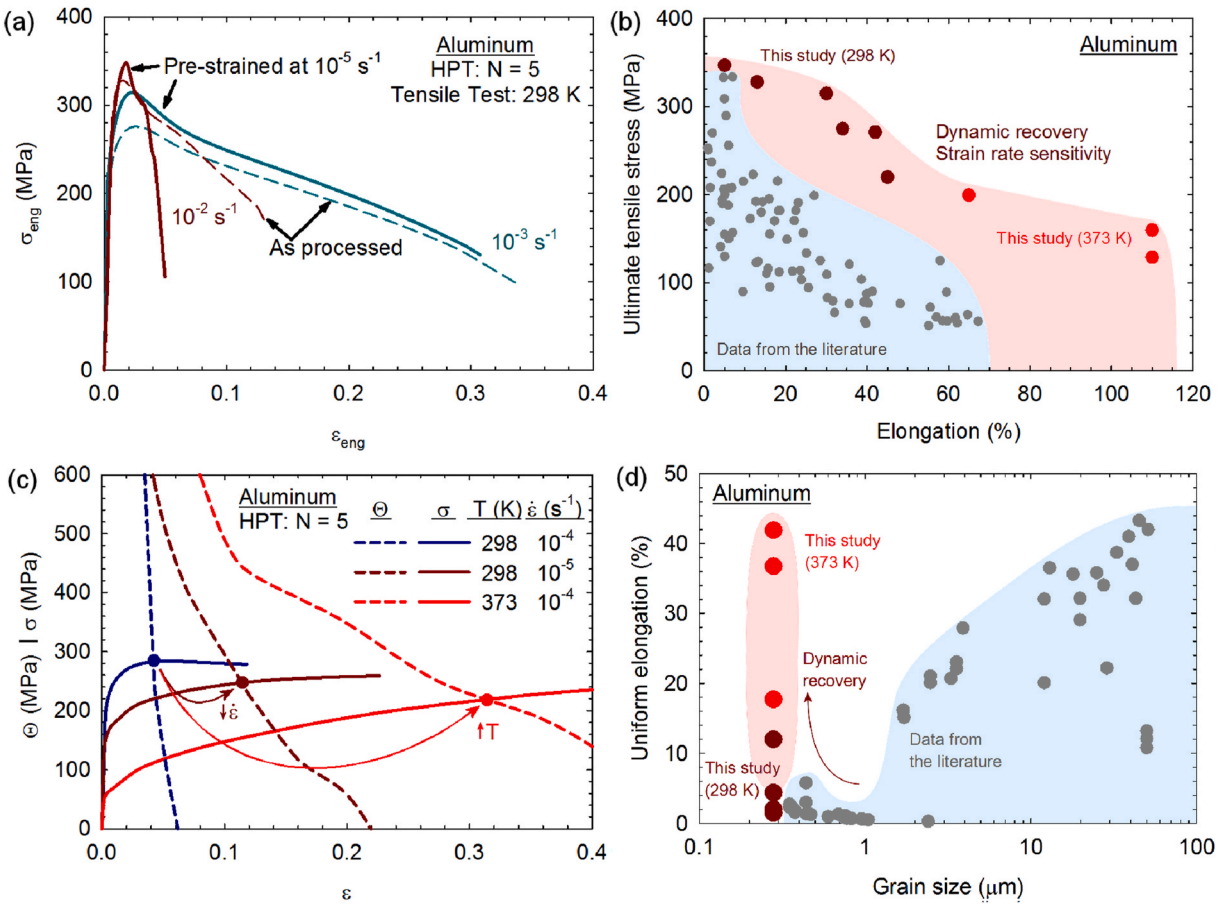

Fig. 9. Dynamic recovery enhanced strength and uniform elongation in nanostructured aluminum. (a) Engineering stress vs. engineering strain curves for tensile tests at high strain rates of nanostructured aluminum with and without pre-straining at a low strain rate. (b) Ultimate tensile strength vs. elongation data from the present study and the literature [10,27–44]. (c) True effective stress and hardening rate vs. effective strain curves for tests at different strain rates and temperatures. (d) Uniform elongation as a function of grain size, including data from the present study and the literature [44,49,50].

enhanced strain rate sensitivity [45], which can stabilize tensile deformation and increase elongation. However, the stabilizing effect from strain rate sensitivity is only observed in the post-uniform range of tensile tests, specifically, during necking. This prevents a severe deformation localization in the necking area, spreading deformation and increasing elongation. The contribution of dynamic recovery is different. It provides hardening during deformation, causing strain-hardening. This effect increases uniform elongation (before necking). The uniform elongation can be estimated at maximum stress in engineering stress vs. strain curves or using the Considère's criterion by the interception of true effective stress vs. strain curves with the hardening curve. This procedure is illustrated in Fig. 9c for three different tests. It is shown that lowering the strain rate decreases the flow stress (as predicted by the grain boundary sliding model) and increases the hardening level. Therefore, the intersection between the curves shifts to larger strain levels. This effect is even more pronounced at a higher temperature. Higher temperatures enhance thermal activation, which reduces the effective stress required for dislocation motion and facilitates dynamic recovery. This effect is comparable to that observed at lower strain rates. Both conditions promote defect annihilation and grain boundary relaxation, which contribute to strain hardening and stabilize plastic deformation, thereby increasing uniform elongation. However, the precise microstructural mechanisms responsible for the observed elongation remain unclear and warrant further investigation. Additional studies focusing on in-situ characterization techniques and advanced modeling are needed to provide direct evidence of these mechanisms.

Strain hardening due to dynamic recovery provides the means to achieve significant levels of uniform elongation in nanostructured aluminum. This is demonstrated in Fig. 9d, which plots the uniform elongation vs. the grain size for aluminum. Data from the literature indicate that negligible uniform elongation is expected for aluminum with grain sizes smaller than ~1 μm. However, the present study shows that dynamic recovery triggered by deformation at low strain rates and higher temperatures can significantly increase the uniform elongation in these materials. This contradicts expectations for coarse-grained materials, where dynamic recovery typically compromises uniform elongation [46]. The present results also show that the flow stress, total elongation and uniform elongation vary significantly with strain rate and temperature in nanostructured materials. Therefore these cannot be considered inherent properties in these materials.

It is important to note the effect of sample size on elongation. Some tests in the literature, and the present study, use miniature samples due to limitations in the dimensions of the processed material. These samples can exhibit large values of post-uniform elongation because the localized deformation (necking) occupy a large fraction of the gauge length. Therefore miniature samples can display larger values of total elongation compared to large counterparts with large gauge length to cross-section ratio. However, the sample size effect is expected to be reduced in the uniform elongation range. In fact experiments on tensile samples with different thicknesses [47,48] reveal that the sample geometry affects the total elongation but there is only minor changes in uniform elongation. This does not compromise the general conclusion of the present study, which is to provide evidence of dynamic recovery as a strengthening mechanism. Although the absolute values of elongation can vary, the fact that deformation-induced hardening occurs at low

strain rates and high temperatures remains valid.

5. Conclusion

In conclusion, the present study demonstrates strain-hardening behavior in nanostructured aluminum during deformation at low strain rates and higher temperatures, conditions that favor dynamic recovery. The microstrain decreases during deformation at a low strain rate, confirming the occurrence of recovery. Strain hardening due to dynamic recovery provides the conditions for achieving uniform elongation in nanostructured aluminum, and this finding is likely extendable to other nanostructured materials. Dynamic recovery strengthening can thus be used to extend the strength-ductility range for nanostructured materials. The concept of "strain-hardening" requires clarification, as it results from defect accumulation in coarse-grained materials but from recovery in nanostructured materials.

Declaration of competing interest

The authors declare that they have no known competing financial interests or personal relationships that could have appeared to influence the work reported in this paper.

Acknowledgments

This research used facilities of the Brazilian Nanotechnology National Laboratory (LNNano), part of the Brazilian Centre for Research in Energy and Materials (CNPEM), a private non-profit organization under the supervision of the Brazilian Ministry for Science, Technology, and Innovations (MCTI). The TEM and SEM/FIB staff are acknowledged for the assistance during the experiments 20230390. The authors acknowledge funding from CNPq-Brazil grants 302832/2022-0 (RBF) and 402634/2023-3 (RBF), FAPEMIG grants BPD-00228-22 (RBF) and APQ-02023-23 (RBF) and National Science Foundation grant CMMI-2051205 (MK). The authors acknowledge the Center for Advanced Research Computing (CARC) at the University of Southern California for providing computing resources that have contributed to the research results reported within this publication. URL: https://carc.usc.edu.

References

[1] Kocks UF, Mecking H. Physics and phenomenology of strain hardening: the FCC case. Prog Mater Sci 2003;48:171–273.
[2] Mungole T, Kumar P, Kawasaki M, Langdon TG. A critical examination of the paradox of strength and ductility in ultrafine-grained metals. J Mater Res 2014;29:2534–46.
[3] Valiev RZ, Alexandrov IV, Zhu YT, Lowe TC. Paradox of strength and ductility in metals processed by severe plastic deformation. J Mater Res 2002;17:5–8.
[4] Ma E, Shen TD, Wu XL. Less is more. Nat Mater 2006;5:515–6.
[5] Liu X, Han J-K, Onuki Y, Kuzminova YO, Evlashin SA, Kawasaki M, et al. In situ neutron diffraction investigating microstructure and texture evolution upon heating of nanostructured CoCrFeNi high-entropy alloy. Adv Eng Mater 2023;25:2201256.
[6] Popov AA, Pyshmintsev IY, Demakov SL, Illarionov AG, Lowe TC, Sergeyeva AV, et al. Structural and mechanical properties of nanocrystalleve titanium processed by severe plastic deformation. Scripta Mater 1997;37:1089–94.
[7] Valiev RZ, Sergueeva AV, Mukherjee AK. The effect of annealing on tensile deformation behavior of nanostructured SPD titanium. Scripta Mater 2003;49:669–74.
[8] Wu S, Kou Z, Lai Q, Lan S, Katnagallu SS, Hahn H, et al. Dislocation exhaustion and ultra-hardening of nanograined metals by phase transformation at grain boundaries. Nat Commun 2022;13:5468.
[9] Gubicza J. Annealing-induced hardening in ultrafine-grained and nanocrystalline materials. Adv Eng Mater 2020;22:1900507.
[10] Huang X, Hansen N, Tsuji N. Hardening by annealing and softening by deformation in nanostructured metals. Science 2006;312:249–51.
[11] Renk O, Maier-Kiener V, Issa I, Li JH, Kiener D, Pippan R. Anneal hardening and elevated temperature strain rate sensitivity of nanostructured metals: their relation to intergranular dislocation accommodation. Acta Mater 2019;165:409–19.
[12] Renk O, Pippan R. Anneal hardening in single phase nanostructured metals. Mater Trans 2023;64:1464–73.
[13] Figueiredo RB, Sabbaghianrad S, Giwa A, Greer JR, Langdon TG. Evidence for exceptional low temperature ductility in polycrystalline magnesium processed by severe plastic deformation. Acta Mater 2017;122:322–31.
[14] Figueiredo RB, Poggiali FS, Silva CL, Cetlin PR, Langdon TG. The influence of grain size and strain rate on the mechanical behavior of pure magnesium. J Mater Sci 2016;51:3013–24.
[15] Carvalho AP, Reis LM, Pinheiro RP, Pereira PHR, Langdon TG, Figueiredo RB. Using plane strain compression test to evaluate the mechanical behavior of magnesium processed by HPT. Metals 2022;12:125.
[16] Thompson AP, Aktulga HM, Berger R, Bolintineanu DS, Brown WM, Crozier PS, et al. Lammps - a flexible simulation tool for particle-based materials modeling at the atomic, meso, and continuum scales. Comput Phys Commun 2022;271:108171.
[17] Mishin Y, Farkas D, Mehl MJ, Papaconstantopoulos DA. Interatomic potentials for monoatomic metals from experimental data and ab initio calculations. Phys Rev B 1999;59:3393–407.
[18] Hirel P. Atomsk: a tool for manipulating and converting atomic data files. Comput Phys Commun 2015;197:212–9.
[19] Stukowski A. Visualization and analysis of atomistic simulation data with OVITO–the Open Visualization Tool. Model Simulat Mater Sci Eng 2010;18:015012.
[20] Zhao YH, Liao XZ, Jin Z, Valiev RZ, Zhu YT. Microstructures and mechanical properties of ultrafine grained 7075 Al alloy processed by ECAP and their evolutions during annealing. Acta Mater 2004;52:4589–99.
[21] Renk O, Hohenwarter A, Eder K, Kormout KS, Cairney JM, Pippan R. Increasing the strength of nanocrystalline steels by annealing: is segregation necessary? Scripta Mater 2015;95:27–30.
[22] Figueiredo RB, Langdon TG. Deformation mechanisms in ultrafine-grained metals with an emphasis on the Hall-Petch relationship and strain rate sensitivity. J Mater Res Technol 2021;14:137–59.
[23] Stukowski A, Bulatov VV, Arsenlis A. Automated identification and indexing of dislocations in crystal interfaces. Model Simulat Mater Sci Eng 2012;20:085007.
[24] Stukowski A, Albe K. Extracting dislocations and non-dislocation crystal defects from atomistic simulation data. Model Simulat Mater Sci Eng 2010;18:085001.
[25] Hasnaoui A, Van Swygenhoven H, Derlet PM. On non-equilibrium grain boundaries and their effect on thermal and mechanical behaviour: a molecular dynamics computer simulation. Acta Mater 2002;50:3927–39.
[26] Renk O, Pippan R. Saturation of grain refinement during severe plastic deformation of single phase materials: reconsiderations, current status and open questions. Mater Trans 2019;60:1270–82.
[27] Karami S, Piroozi B, Borhani E. Fatigue-induced microstructure evolution and ratcheting behavior of ultrafine-grained (UFG) pure aluminum processed by accumulative roll bonding (ARB). Mater Char 2023;196:112578.
[28] Zhao YH, Bingert JF, Topping TD, Sun PL, Liao XZ, Zhu YT, et al. Mechanical behavior, deformation mechanism and microstructure evolutions of ultrafine-grained Al during recovery via annealing. Materials Science and Engineering: A. 2020;772:138706.
[29] Kamikawa N, Hirooka T, Furuhara T. Yielding behaviour and Hall–Petch relationship in ultrafine-grained Al–Mg binary alloys. Mater Sci Technol 2021;37:210–23.
[30] Wang BB, Xie GM, Wu LH, Xue P, Ni DR, Xiao BL, et al. Grain size effect on tensile deformation behaviors of pure aluminum. Materials Science and Engineering: A. 2021;820:141504.
[31] Su L, Lu C, Li H, Deng G, Tieu K. Investigation of ultrafine grained AA1050 fabricated by accumulative roll bonding. Materials Science and Engineering: A. 2014;614:148–55.
[32] Zeng W, Shen Y, Zhang N, Huang X, Wang J, Tang G, et al. Rapid hardening induced by electric pulse annealing in nanostructured pure aluminum. Scripta Mater 2012;66:147–50.
[33] Kamikawa N, Huang X, Tsuji N, Hansen N. Strengthening mechanisms in nanostructured high-purity aluminium deformed to high strain and annealed. Acta Mater 2009;57:4198–208.
[34] Raab GJ, Valiev RZ, Lowe TC, Zhu YT. Continuous processing of ultrafine grained Al by ECAP–Conform. Materials Science and Engineering: A. 2004;382:30–4.
[35] Azimi A, Tutunchilar S, Faraji G, Besharati Givi MK. Mechanical properties and microstructural evolution during multi-pass ECAR of Al 1100–O alloy. Mater Des 2012;42:388–94.
[36] Pirgazi H, Akbarzadeh A, Petrov R, Kestens L. Microstructure evolution and mechanical properties of AA1100 aluminum sheet processed by accumulative roll bonding. Materials Science and Engineering: A. 2008;497:132–8.
[37] Höppel HW, May J, Göken M. Enhanced strength and ductility in ultrafine-grained aluminium produced by accumulative roll bonding. Adv Eng Mater 2004;6:781–4.
[38] Jafarzadeh H, Abrinia K. Fabrication of ultra-fine grained aluminium tubes by RTES technique. Mater Char 2015;102:1–8.
[39] Orlova TS, Sadykov DI, Kirilenko DA, Lihachev AI, Levin AA. The key role of grain boundary state in deformation-induced softening effect in Al processed by high pressure torsion. Materials Science and Engineering: A. 2023;875:145122.
[40] Zhao Y, Li L, Lu Z, Teng G, Liu S, Hu Z, et al. The effect of annealing temperature on the recrystallization and mechanical properties of severe plastic deformed commercial pure aluminium during ultra-fast annealing. Mater Res Express 2021;8:046515.
[41] Abd El Aal MI, Sadawy MM. Influence of ECAP as grain refinement technique on microstructure evolution, mechanical properties and corrosion behavior of pure aluminum. Trans Nonferrous Metals Soc China 2015;25:3865–76.
[42] Orlova TS, Mavlyutov AM, Gutkin MY. Suppression of the annealing-induced hardening effect in ultrafine-grained Al at low temperatures. Materials Science and Engineering: A. 2021;802:140588.

[43] Chen X, Huang G-S, Liu S-S, Han T-Z, Jiang B, Tang A-T, et al. Grain refinement and mechanical properties of pure aluminum processed by accumulative extrusion bonding. Trans Nonferrous Metals Soc China 2019;29:437–47.
[44] Bhatta L, Lee I, Figueiredo RB, Bay BK, Kawasaki M. Digital image correlation analysis of uniform deformation and necking in solid-state welded nanocrystalline aluminum via high-pressure torsion.Adv Eng Mater.n/a:2400439.
[45] Figueiredo RB, Kawasaki M, Langdon TG. Seventy years of Hall-Petch, ninety years of superplasticity and a generalized approach to the effect of grain size on flow stress. Prog Mater Sci 2023;137:101131.
[46] Yasnikov IS, Vinogradov A, Estrin Y. Revisiting the Considère criterion from the viewpoint of dislocation theory fundamentals. Scripta Mater 2014;76:37–40.
[47] Yuan WJ, Zhang ZL, Su YJ, Qiao LJ, Chu WY. Influence of specimen thickness with rectangular cross-section on the tensile properties of structural steels. Materials Science and Engineering: A. 2012;532:601–5.
[48] Takeda Y, Kiattisaksri C, Aramaki M, Munetoh S, Furukimi O. Effects of specimen thickness in tensile tests on elongation and deformation energy for industrially pure iron. ISIJ Int 2017;57:1129–37.
[49] Kamikawa N, Hirochi T, Furuhara T. Strengthening mechanisms in ultrafine-grained and sub-grained high-purity aluminum. Metall Mater Trans 2019;50:234–48.
[50] Yu CY, Kao PW, Chang CP. Transition of tensile deformation behaviors in ultrafine-grained aluminum. Acta Mater 2005;53:4019–28.